

## Observation of charge enhancement induced by graphite atomic vacancy: A comparative STM and AFM study

J. R. Hahn and H. Kang\*

*Department of Chemistry, Pohang University of Science and Technology, Pohang, Gyeongbuk, Korea 790-784*

S. Song and I. C. Jeon

*Department of Chemistry, Jeonbuk National University, Jeonbuk, Korea 560-756*

(Received 21 September 1995)

An atomic vacancy is produced on a graphite surface by bombarding it with low-energy (40–80 eV) beams of  $\text{Ar}^+$  ions, and its structure is examined by scanning tunneling microscopy (STM) and atomic force microscopy (AFM). The atomic vacancy is imaged as a surface protrusion in STM, while it is transparent in AFM. These two contradictory results are explained by the vacancy-induced enhancement of the partial charge density of states at the carbon atoms near the vacancy. The charge enhancement can occur over tens of the surrounding carbon atoms for multiatom vacancy.

Physical properties of solids can be affected profoundly by the presence of defects in the solid. An atomic vacancy, consisting of the absence of one or a few atoms, provides the simplest example of deviation from perfect crystal behavior. Yet, only limited information has been revealed about its structure. With the advent of scanning probe microscopy (SPM), it has become possible to directly examine vacancies on a surface. SPM, being a near field and real-space probe, has its merits for investigating the defects of atomic scale and of random spatial distribution. SPM study of layered materials has another advantage. Since graphite is basically a two-dimensional solid, with strong covalent bonding in two-dimensional layers and only weak van der Waals interactions holding the layers together, structure and electronic properties revealed by the surface-sensitive technique will mostly resemble those in the bulk.

In principle, an atomic vacancy can be generated by removing surface atoms with energetic particle bombardment. High-energy ( $> \text{keV}$ ) ion beams, however, cause severe damage to a surface such as large craters and extensive structural disorder. Such high-energy damage has been studied using scanning tunneling microscopy (STM) and atomic force microscopy (AFM) on various materials.<sup>1–7</sup> When the ion impact energy is very low ( $< 100 \text{ eV}$ ), i.e., in the regime of atomic displacement threshold, the impinging ions remove one or at most a few surface atoms, and thus produce atomic vacancy.<sup>8–12</sup> Recently, several researchers have reported STM images of the defected graphite surfaces prepared using low-energy ions,<sup>8,12,13</sup> which show protrusions of a few Å in diameter that can be recognized as point defects. It remains controversial, though, how these STM features should be interpreted because STM probes tunneling current rather than actual surface topography. In an attempt to disentangle the electronic and lattice effects, we have produced defects on graphite with  $\text{Ar}^+$  beams of various energies, and examined their structure using both STM and AFM. We find that the STM protrusions originate from an increased partial charge density near the Fermi level ( $E_F$ ), although the actual topography at a vacancy site is almost flat.

Graphite samples, (HOPG, Union Carbide ZYA grade)

were cleaved perpendicular to the  $c$  axis just before loading into the ion-surface collision apparatus. This instrument consists of an ion source, beam transport region, low-energy decelerator, and ultrahigh vacuum (UHV) sample chamber equipped with surface analysis tools.<sup>14</sup> The sample was bombarded with mass- and energy-selected  $\text{Ar}^+$  ion beams in the energy range 40–80 eV. This energy region was chosen because the thresholds for surface penetration and atomic displacement lie between 40 and 50 eV for the  $\text{Ar}^+$  graphite system.<sup>9,11</sup> Any neutral species contained in the beam were removed by a  $12^\circ$  electrostatic deflection. Differential pumping of the beam line allows us to maintain the pressure of the sample chamber below  $2 \times 10^{-9}$  Torr during beam exposure. The energy resolution for the low-energy beam was 2 eV full width at half maximum. The beam dose was kept low ( $< 5 \times 10^{13}$  ions/cm<sup>2</sup>), so that the effects of single knock-on events can be isolated on the surface. The beam collided with a surface in the normal direction and was rastered over the target area for uniform exposure. No surface impurity species were found before and after beam exposure as checked by Auger electron spectroscopy (AES). The sample was then transferred to STM and AFM instrumental stages operated in air for subsequent measurements.

STM measurements were done using a home-built instrument and a commercially available one.<sup>15</sup> Mechanically cut Pt-Ir and electrochemically etched W wires were used for the tip. The tip was made sure to give atomic resolution on the undamaged surface both before and after scanning over the defect structures. The defect image was optimal under low bias voltage (20–100 mV) and low tunneling resistance conditions ( $10^8 \Omega$ ). Force measurements were performed using two types of scanning force microscopy,<sup>15</sup> one operating in the contact constant height mode (AFM) and another in the lateral force mode (LFM). Both instruments were equipped with a 5- $\mu\text{m}$  scanner calibrated using a mica sample and a commercial silicon nitride cantilever of a force constant  $0.6 \text{ N m}^{-1}$ . The AFM scan rates were typically 10–25 Hz, and the applied forces ranged between 0.4 and 100 nN.

Figure 1 presents the STM and AFM images obtained from a sample bombarded with 80-eV  $\text{Ar}^+$  ions. The STM

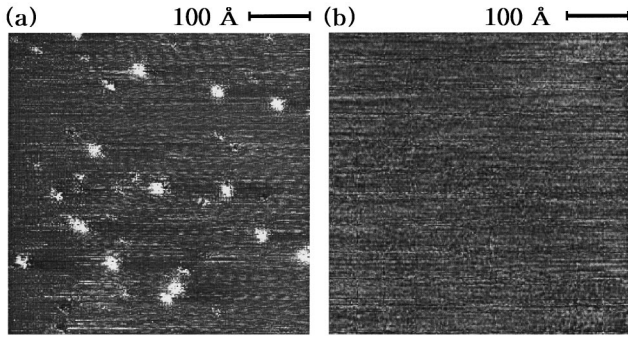


FIG. 1. (a) STM image obtained from an area of  $500 \times 500 \text{ \AA}^2$  of a graphite surface bombarded with 80-eV  $\text{Ar}^+$  ions. Constant height mode with a scan rate of 12 Hz, sample bias of 160 mV, and tunneling current of 0.5 nA. (b) The AFM image of  $500 \times 500 \text{ \AA}^2$  from the same graphite surface. The scan rate is 12.5 Hz and the force 20 nN.

image [Fig. 1(a)] shows protrusions (bright spots) dispersed randomly on the originally flat area of  $500 \times 500 \text{ \AA}^2$ . Images similar to this have been reported in the previous STM studies of ion-impacted graphite,<sup>8,13</sup> and each protrusion is interpreted as the signature of individual ion impact. The size of the hillocks varies from a few to tens of  $\text{\AA}$  in diameter, although the small ones are almost invisible in this wide-scan image. On the other hand, the corresponding AFM image shown in Fig. 1(b) appears nearly flat and free of these structures. These two contrasting results must be related to the fact that STM and AFM probe different properties of a surface; the STM image is described by the partial electron density near the Fermi level ( $E_F$ ) while the AFM image corresponds to surface topography or the total electron density plot.<sup>16</sup>

Although SPM is a powerful technique for imaging local defects, a rational interpretation of its image is often not straightforward and can be greatly assisted if supporting information is available. We can obtain a useful guideline for interpretation of the present data by examining the effect of incident beam energy on defect production. In this experiment, we have taken about 300 STM images for each beam energy (40, 50, 60, and 80 eV) in order to get good statistics for the defect features, and the results are summarized in Table I. Upon bombardment of 40-eV  $\text{Ar}^+$ , no STM protrusion is observed and the surface remains the same as the original state. Since STM can detect atomic vacancies as well as bulges on the surface caused by trapping Ar atoms underneath the top graphite layer,<sup>8,12</sup> this observation means that 40-eV  $\text{Ar}^+$  ions do not produce a surface vacancy or

TABLE I. Statistical results of the STM image analysis for various  $\text{Ar}^+$  impact energies.

Ion energy, eV	40	50	60	80
Diameter of the protrusion in $\text{\AA}$ : average value (distribution range)	0	6.3 (2–12)	8.1 (2–16)	13.1 (2–30)
Height of protrusion in $\text{\AA}$ : average value (distribution range)	0	1.4 (0.8–7)	2.1 (0.8–7)	3.5 (0.8–9)

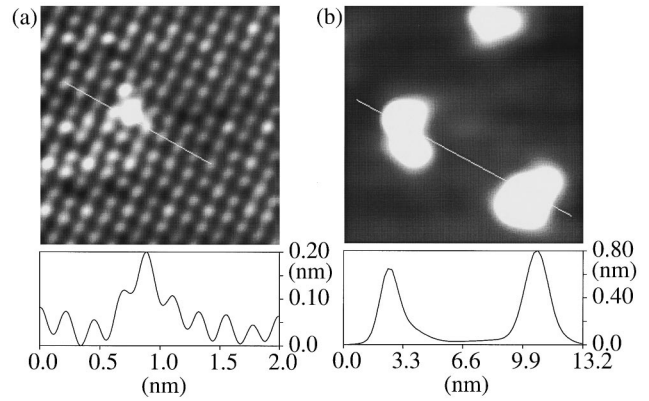


FIG. 2. Constant-current STM images of graphite surfaces bombarded with 60-eV (a) and 80-eV  $\text{Ar}^+$  ions (b). The lower boxes show cross-sectional intensity along the lines marked on the images. These are unfiltered raw images. The trigonal pattern of a graphite lattice is distorted in Fig. 2(a) due to upward thermal drift. Scan conditions are (a) sample bias of  $-36$  mV, tunneling current of 0.5 nA, and scan rate of 10 Hz; (b) sample bias of  $-30$  mV, tunneling current of 0.5 nA, and scan rate of 3 Hz.

penetrate a surface. Small hillocks start to appear at the impact energy of 50 eV, a value only a few eV higher than the threshold energies reported in the literature,<sup>9,11</sup> the threshold for  $\text{Ar}^+$  penetration into the first graphite layer has been reported to be  $43.5 \pm 1.5$  eV from AES line-shape analysis<sup>11</sup> and 42 eV from our classical trajectory simulation (CTS).<sup>9</sup> According to the CTS,<sup>9</sup> the Ar projectile can penetrate through the center of a hexagonal carbon ring at this lowest energy without permanently displacing surface carbon atoms. The threshold for carbon atom displacement or vacancy formation is slightly higher, and a value of 47.3 eV has been obtained from the AES study.<sup>9</sup> With the average vacancy formation energy of 7.44 eV for graphite,<sup>17</sup> 50-eV  $\text{Ar}^+$  beams can remove at most one surface carbon, thus producing only single-atom vacancy. Indeed, the STM hillocks of smallest sizes (2–7  $\text{\AA}$  in diameter) appear at this energy, which should be originating from the single-atom vacancy.

With increasing ion energy, larger-size protrusions are more frequently observed by STM. The average diameter and height of the protrusions continuously increase with energy. The average diameters are 6.3  $\text{\AA}$  (50 eV), 8.1  $\text{\AA}$  (60 eV), and 13.1  $\text{\AA}$  (80 eV), and the average heights 1.4  $\text{\AA}$  (50 eV), 2.1  $\text{\AA}$  (60 eV), and 3.5  $\text{\AA}$  (80 eV). The average numbers of carbon atoms inside the protruded area are 12, 19, and 52 atoms for the energies of 50, 60, and 80 eV, respectively. Upon higher energy collisions ( $>60$  eV), more than one surface carbon can be removed, but there is an energetic limit for the number of missing atoms which is four even at the highest collision energy (80 eV). This maximum number applies only to the ideal or most favorable collision-induced ejection. Therefore, it is apparent that the observed STM protrusion is much larger than a possible vacancy size.

Figure 2(a) presents an example of high-resolution, constant-current STM image for the defect feature which we assign as a single-atom vacancy. The small hillock of this image is the predominant structure produced upon 50–60-eV  $\text{Ar}^+$  impact. The cross-sectional cut of the image, shown at the bottom of Fig. 2(a), reveals its size to be 5  $\text{\AA}$  in diameter and 1.5  $\text{\AA}$  in height. Except in this locally bright area, the

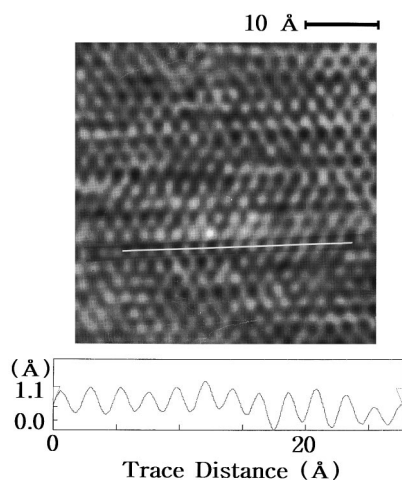


FIG. 3. AFM image of a surface bombarded with 60-eV  $\text{Ar}^+$  ions [the same surface as Fig. 2(a)]. The cross-sectional topography along the trace is shown at the bottom. The scan rate is 25 Hz with the force 35.2 nN. The image has been low-pass filtered.

surface resembles the original graphite structure. Typical large-size hillocks produced by an 80-eV collision are shown in Fig. 2(b). The protrusions have diameters of 14–17 Å and heights of 6–7 Å, as indicated at the bottom of Fig. 2(b). These high protrusions make the rest of the surface appear relatively dark and flat in the image of Fig. 2(b), but the original graphite pattern is still retained in this flat region as checked from its zoomed images.

Figure 3 exemplifies an AFM image of the surface bombarded with 60-eV  $\text{Ar}^+$  ions. In contrast to STM, AFM images of the ion-bombarded surfaces do not show any protrusions or depressions of a significant degree. The image appears relatively flat showing only the atomic corrugation of graphite lattice. Such a degree of corrugation is similar to or slightly increased ( $<10\%$ ) from the original state. No direct sign of vacancy can be observed with AFM and LFM even when atomic structure can be resolved on the surface. This is probably due to intrinsically lower sensitivity of these force microscopies for imaging randomly distributed, atomic-scale defects, because a tip-sample interaction area is larger in the force microscopies than in STM. To our knowledge, AFM studies have reported the images of large-scale defects<sup>6,18</sup> and line defects,<sup>19</sup> but direct imaging of atomic vacancy has been rather unsuccessful.<sup>20</sup> Fourier transformation of the present AFM images reveals that the hexagonal spots in the reciprocal lattice space become slightly blurred and weaker after ion impact. Such a change in the Fourier-transformed images suggests some deterioration in the long-range hexagonal periodicity of the surface, therefore implying defect creation by ions.

Since the carbon atoms adjacent to an atomic vacancy have dangling bonds, it may be possible that some impurity molecules are bonded to them under ambient conditions. LFM is currently regarded as the best means for imaging soft molecules adsorbed on a surface.<sup>18,21</sup> LFM investigations<sup>18</sup> for the large-scale damage generated by high-energy ( $> \text{keV}$ ) ion bombardment show remarkably increased friction inside the damaged zone of about 100 Å in diameter, which has been attributed to the higher lateral force acting on the tip introduced by water or other molecules chemisorbed

on the damaged surface. On the 50–80-eV ion-bombarded surfaces, on the other hand, we do not detect any substantial change in the lateral forces. This LFM observation suggests either that molecules do not adsorb on an atomic vacancy or that the adsorption is localized only to the vacancy region of a size of less than a few atoms, thereby contributing undetectable adsorbate friction. A consistent interpretation can be reached from the STM observation that the protrusions do not change their shape upon many repeated scans. The molecular adsorbates would become substantially modified by the STM tip-surface interactions in the present tunneling resistance condition ( $10^8 \Omega$ ). Therefore, we conclude that the adsorbate effect is either absent or relatively negligible, at least for the large STM features.

The large STM protrusions, exemplified in Fig. 2(b), best illustrate the difference between the STM and AFM results. The protrusion covers an area of several tens of carbon atoms, despite the fact that the maximum vacancy size attainable is only a few missing atoms at these impact energies. A most feasible explanation for these protrusions is found from the electronic structure calculations for graphite atomic vacancy,<sup>17,22</sup> which predict that the charge density of states (CDOS) is increased in the carbon atoms surrounding an atomic vacancy both in their filled and empty states near  $E_F$ . The present STM and AFM results agree well with this calculated electronic structure; since the STM image of a surface is described by the partial CDOS plot near  $E_F$ ,  $\rho(r, E_F)$ ,<sup>16</sup> STM can efficiently monitor the CDOS change in the neighboring carbons introduced by the vacancy. On the other hand, AFM probes topography, i.e., the total charge density contour  $\rho(r)$  of a surface. In this case the vacancy-induced partial CDOS change is not necessarily detected by AFM, as long as the total charge density is not changed substantially. When we changed the bias voltage between an STM tip and a sample, we found that low bias voltages ( $<100 \text{ mV}$ ) produced the best contrast for the protrusion. Reversing the bias polarity did not noticeably change the image quality. Such bias dependency is also consistent with the CDOS increase close to  $E_F$ . One might expect some electronic perturbations of the surface introduced by impurity adsorption. However, the resulting charge enhancement is unlikely to become significant, because electronegativity of water or common organic adsorbates is higher than a graphite surface.<sup>23</sup>

According to the theoretical calculation,<sup>17</sup> the CDOS enhancement effect increases with the size of a graphite vacancy. We observe larger STM protrusions with higher frequency upon higher-energy collisions. As it is energetically feasible to remove more than one surface carbon at high energies (60–80 eV), we attribute the large protrusion to a CDOS increase coming from the multiatom vacancy. Although quantitative information on the charge distribution is only remotely possible from the STM data alone, Fig. 2(b) clearly shows that the CDOS is increased over tens of the surrounding surface atoms. The small STM hillocks of 2–7 Å in diameter, on the other hand, are attributed to a single-atom vacancy as they are the features most frequently produced under conditions of single-atom ejection. The area of these small features encompasses 3–15 carbon atoms, which correspond to the first- or second-nearest-neighbor carbons. This may represent the charge enhancement range of a

single-atom vacancy, provided that the adsorbate effects can be neglected for these small features as well.

We conclude from the present STM and AFM study that the atomic vacancy created by low-energy Ar<sup>+</sup> impact on a graphite surface results in a CDOS increase at the surrounding carbon atoms. This CDOS increase appears to be concentrated near  $E_F$ , thus producing a hillock structure in STM while it is transparent in AFM. The single-atom vacancy produces a hillock structure of a few Å in diameter in STM.

Higher-energy (60–80-eV) collision often produces a hillock structure encompassing several tens of surface atoms, representing rather large electronic perturbations of the surface. This large structure cannot be due to surface adsorbates.

This work was supported in part by the Non-directed Research Fund from Korea Research Foundation, Center for Molecular Science, and the Ministry of Education of Korea (Grants Nos. BSRI-94-3430 and 94-3438).

- 
- \*Author to whom correspondence should be addressed. FAX: 82-562-279-3399. Electronic address: surfion@vision.postech.ac.kr
- <sup>1</sup>R. M. Feenstra and G. S. Oehrlein, *Appl. Phys. Lett.* **47**, 97 (1985).
- <sup>2</sup>I. H. Wilson, N. J. Zheng, U. Knipping, and I. S. T. Tsong, *Phys. Rev. B* **38**, 8444 (1988).
- <sup>3</sup>L. Porte, C. H. de Villeneuve, and M. Phaner, *J. Vac. Sci. Technol. B* **9**, 1064 (1991).
- <sup>4</sup>R. Coratger, A. Claverie, A. Chahboun, V. Landry, F. Ajustron, and J. Beauvillain, *Surf. Sci.* **262**, 208 (1992).
- <sup>5</sup>E. J. Snyder and R. S. Williams, *Surf. Sci.* **285**, 157 (1993).
- <sup>6</sup>F. Thibaudau, J. Cousty, E. Balanzat, and S. Bouffard, *Phys. Rev. Lett.* **67**, 1582 (1991).
- <sup>7</sup>T. Li, B. V. King, R. J. MacDonald, G. F. Cotterill, D. J. O'Connor, and Q. Yang, *Surf. Sci.* **312**, 399 (1994).
- <sup>8</sup>H. Kang, K. H. Park, C. Kim, B. S. Shim, S. Kim, and D. W. Moon, *Nucl. Instrum. Methods B* **67**, 312 (1992).
- <sup>9</sup>W. Choi, C. Kim, and H. Kang, *Surf. Sci.* **281**, 323 (1993).
- <sup>10</sup>H. J. Steffen, D. Marton, and J. W. Rabalais, *Phys. Rev. Lett.* **68**, 1726 (1992).
- <sup>11</sup>D. Marton, K. J. Boyd, T. Lytle, and J. W. Rabalais, *Phys. Rev. B* **48**, 6757 (1993).
- <sup>12</sup>D. Marton, H. Bu, K. J. Boyd, S. S. Todorov, A. H. Al-Bayati, and

- J. W. Rabalais, *Surf. Sci.* **326**, L489 (1995).
- <sup>13</sup>G. M. Shedd and P. E. Russell, *J. Vac. Sci. Technol. A* **9**, 1261 (1991).
- <sup>14</sup>K. H. Park, B. K. Kim, and H. Kang, *J. Chem. Phys.* **97**, 2742 (1992).
- <sup>15</sup>AutoProbe LS and CP, Park Scientific Instruments.
- <sup>16</sup>S. N. Magonov and M. Whangbo, *Adv. Mater.* **6**, 355 (1994).
- <sup>17</sup>K. H. Lee, H. M. Lee, H. M. Eun, W. R. Lee, S. Kim, and D. Kim, *Surf. Sci.* **321**, 267 (1994).
- <sup>18</sup>T. Hagen, S. Grafström, J. Ackermann, R. Newmann, C. Trautmann, J. Vetter, and N. Angert, *J. Vac. Sci. Technol. B* **12**, 1555 (1994).
- <sup>19</sup>O. Nickolayev and V. F. Petrenko, *J. Vac. Sci. Technol. B* **12**, 2443 (1994).
- <sup>20</sup>A. L. Shluger, R. M. Wilson, and R. T. Williams, *Phys. Rev. B* **49**, 4915 (1994).
- <sup>21</sup>H. Wolf, H. Ringsdorf, E. Delamarche, T. Takami, H. Kang, B. Michel, Ch. Gerber, M. Jaschke, H.-J. Butt, and E. Mamberg, *J. Phys. Chem.* **99**, 7102 (1995).
- <sup>22</sup>M. R. Soto, *J. Microsc.* **152**, 779 (1988).
- <sup>23</sup>H. Brune, J. Winterlin, J. Trost, G. Ertl, J. Wiechers, and R. J. Behm, *J. Chem. Phys.* **99**, 2128 (1993).